State-selective electron capture in $^3He^{2+}$ + He collisions at intermediate impact energies

M. Alessi,[1,2] S. Otranto,[3] and P. Focke[2]

[1]*Instituto Balseiro, Av. E. Bustillo 9500, 8400 San Carlos de Bariloche, Argentina*

[2]*Centro Atómico Bariloche, Av. E. Bustillo 9500, 8400 San Carlos de Bariloche, Argentina*

[3]*CONICET and Departamento de Física Universidad Nacional del Sur, Av. Alem 1253, 8000 Bahía Blanca, Argentina*

(Received 22 September 2010; published 14 January 2011)

In this work we have measured single-electron capture in collisions of $^3He^{2+}$ projectiles incident on a helium target for energies of 13.3–100 keV/amu with the cold-target recoil-ion momentum spectroscopy setup implemented at the Centro Atómico Bariloche. State-selective single-capture cross sections were measured as a function of the impact energy. They were found to agree with previous existing data from the Frankfurt group, starting at the impact energy of 60 keV/amu; as well as with recent data, at 7.5 keV/amu, from the Lanzhou group. The present experimental results are also contrasted to the classical trajectory Monte Carlo method with dynamical screening.

DOI: 10.1103/PhysRevA.83.014701 PACS number(s): 34.70.+e, 34.50.Bw

During the past 15 years, the incorporation of the cold-target recoil-ion momentum spectroscopy (COLTRIMS) method in several laboratories worldwide has led to an important advance in the experimental studies of atomic and molecular collisions [1–9]. This method allows the measurement of collision events at the fully differential level, providing, in this sense, an unprecedented kinematically complete physical picture for several collision processes. As a result, a large number of studies concerning charge exchange and atomic single and double ionization by ions, electrons, and photons, among other processes, have been performed, renewing interest in the atomic and molecular collision processes [7,10–12].

Charge-exchange processes involving atomic targets have been thoroughly investigated theoretically, as well as experimentally, during the past decades [6,13–20]. However, most of these experiments were focused on obtaining the total cross sections and only in a few cases studies were made in order to determine the different state-selective capture cross sections [13–15,21–23]. Within the COLTRIMS method, the use of the recoil-ion momentum spectroscopy technique provides direct access to the projectile energy transfer during the process of interest. From the recoil-ion longitudinal momentum distribution, state-selective capture cross sections for the present collision system can be obtained as done by Mergel *et al.* [21] (for collision energies in the range 60–250 keV/amu) and more recently by Zhu *et al.* at (7.5 keV/amu) [9].

In this work, we show the results obtained using the Kevatron accelerator at the Centro Atómico Bariloche together with our COLTRIMS setup for single charge-exchange processes in $^3He^{2+}$+He collisions. The range of impact energies considered was 13.3–100 keV/amu. We present state-selective cross sections as a function of the impact energy and compare them at the edges of our measured energies with the available data from the Frankfurt and Lanzhou groups.

Let us now briefly describe our experimental setup. The Kevatron accelerator at the Centro Atómico Bariloche is a Cockroft-Walton machine that operates in the range 20–300 kV. The projectile beam is magnetically analyzed by a 90° bending magnet and collimated by two sets of adjustable slits to a beam cross section of $0.5 \times 0.5\ mm^2$ before entering the collision chamber. In the collision chamber the projectiles cross the recoil-ion spectrometer in which an electrostatic field, transverse to the projectile beam, extracts the recoil ions produced in the collision and accelerates them during the first 40 mm. To this acceleration region, in the spectrometer, follows a field-free drift of 80 mm. The recoil ions produced in the collision region hit a position and time-sensitive microchannel-plate (MCP) detector of 40 mm diameter [24]. This spectrometer configuration allows for time-focusing [25] operation. Typical electric fields used were of 3.75 V/cm. The target is supplied by a supersonic gas jet, produced with a nozzle with a 30 μm opening followed by a skimmer of 0.3 mm diameter. The nozzle-to-skimmer distance used was nearly 13 mm. The driving pressure used was 2 bar and we achieved a gas-jet diameter of 1.4 mm in the collision region and a jet density of 7.8×10^{11} atoms/cm^3. The projectiles leaving the collision chamber pass through an electrostatic deflector that separates the different charge states. The selected charged projectiles are detected by a set of two Channeltron detectors and measured in coincidence with the recoil ions. A more detailed description of the experimental procedure and the equipment configuration can be found in Ref. [26].

Along the projectile beam axis, energy and momentum conservation lead to the following relation (in atomic units) for charge exchange processes [16,17]:

$$p_l = -\left(\frac{Q}{v_p}\right) - \frac{n_e v_p}{2}. \tag{1}$$

Here the Q factor is given by the inelasticity of the reaction (i.e., the difference between the initial and the final sum over all electronic binding energies), v_p is the projectile velocity, and n_e is the number of electrons transferred from the target to the projectile. The first term in Eq. (1) reflects the momentum change of the projectile, and the second term reflects the mass transfer from the target to the projectile.

In contrast to ionization processes, where the p_l distribution is given by a smooth structure starting in an abrupt rise corresponding to the electron capture to the continuum (ECC) mechanism, charge-exchange processes lead to discrete values of p_l [27]. As a result, the obtained distributions not only reflect the way in which the different final states of the projectile are populated by the captured electrons but are also determined by the electronic final state of the remaining target core. Since the target has two electrons in its initial state, once the first

electron is captured either to the ground or an excited state, there still remains the possibility that the second electron could be found in an excited state of the target. In the following, we use the same notation as Mergel *et al.* [21] to refer to the projectile-target final electronic states. The case in which the target and the projectile end up with one electron in the ground state each will be denoted (1,1). In this notation, the first element is given by the n value of the captured electron while the second element is given by the n' value of the electron which remains bound to the target. Events where the projectile and/or the target are in different excited states will be identified by using a similar notation, that is (1,2) & (2,1),(1,$\geqslant$3) & ($\geqslant$3,1),($\geqslant$2,$\geqslant$2).

The present experimental data are contrasted with classical trajectory Monte Carlo simulations in which the Hamilton equations for the classical four-body system are numerically solved. Due to the instability of the classical He atom, four-body CTMC codes generally employ one of the following strategies. (a) In the Bohr atom strategy [28], the explicit $1/r_{12}$ interaction is considered and the electrons are located in circular orbits with opposite momentum at equal distances from the nucleus, which lies right between the electrons. In some cases stabilizing potentials or Heisenberg cores are also employed [29]. (b) In the split-shell model [30], the interelectronic interaction $1/r_{12}$ is neglected during the whole collision process and the bound electrons are initialized with the corresponding sequential binding energies. (c) The dCTMC model [31,32] considers a dynamical screening for the electrons that depends on their binding energies. In this sense, the dCTMC model incorporates radial correlation among the initially bound electrons (without the risk of nonphysical autoionization) at the expense of sacrificing the angular correlation [31,32]. Since single capture together with excitation provides a good fraction of the total single charge-exchange events recorded and electronic correlation is expected to play a role, dCTMC results will be contrasted against the present data.

As usual, the classical number n_c is obtained from the binding energy E_p of the electron relative to the projectile by

$$E_p = -Z_p^2/\left(2n_c^2\right), \tag{2}$$

where Z_p is the charge of the projectile. Then, n_c is related to the quantum number n of the final state by the Becker and McKellar condition [33],

$$[(n-1)(n-1/2)n]^{1/3} \leqslant n_c \leqslant [n(n+1)(n+1/2)]^{1/3}. \tag{3}$$

Similar exit tests were performed for both electrons on those events corresponding to single charge exchange. This procedure allowed the identification of the n-values of each electron with respect either to the projectile or the remaining target core according to their final binding energies.

In Figs. 1(a)–1(d) we show the measured p_l distributions for single-capture collisions for projectile impact energies of 13.3, 20, 25, and 66.67 keV/amu, respectively. The different peaks relate to different energy changes of the projectile in concordance with Eq. (1). As can be seen, all distributions shown are mainly composed of a two-peak structure that is now described. The peak on the left corresponds to a single charge-exchange process in which the target and projectile end up with one electron in the ground state each [i.e., (1,1)]. The peak on the right is built upon the contributions of the following

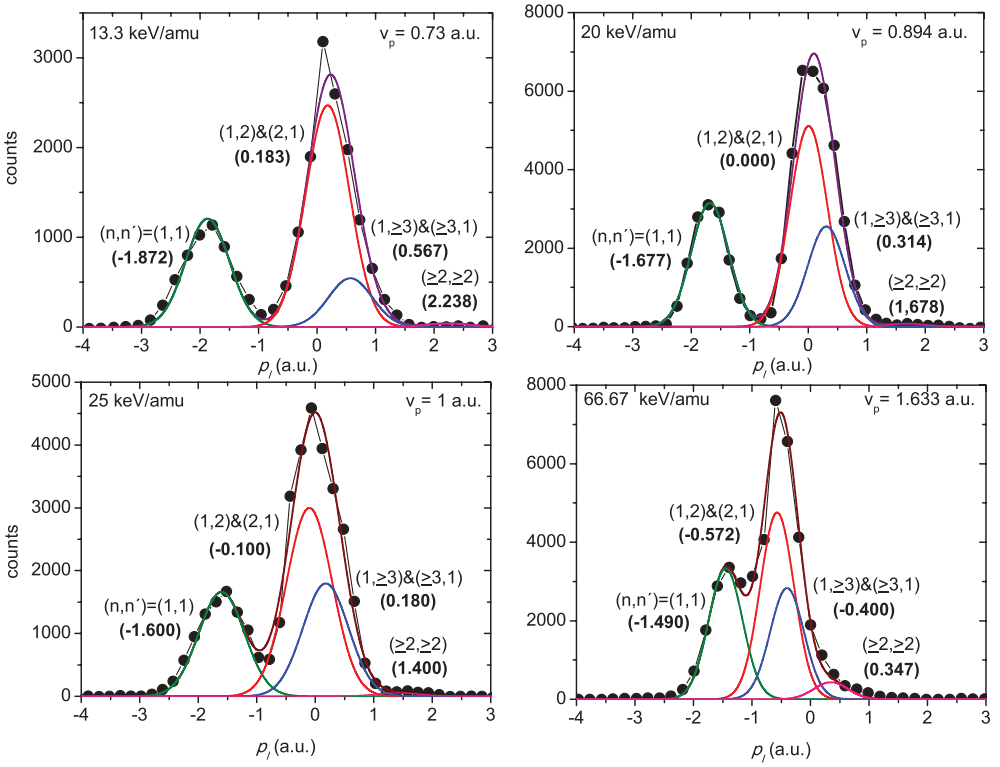

FIG. 1. (Color online) Longitudinal momentum distribution for He^+ recoil ions from the 40, 60, 75, and 200-keV $^3He^{2+}+He \rightarrow {}^3He^+ + He^+$ reactions (one electron capture). The numbers within brackets represent the expected p_l value according to Eq. (1).

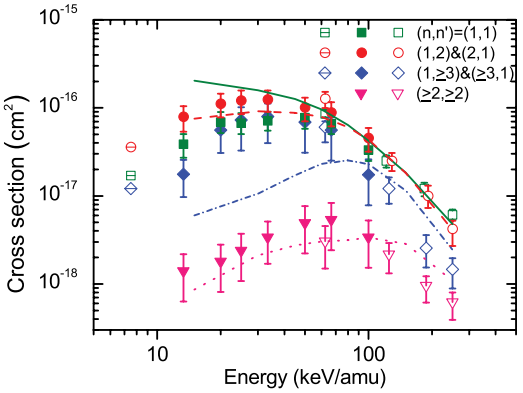

FIG. 2. (Color online) State-selective capture cross sections as indicated in the figure. Solid symbols, this work; open symbols, data from Mergel *et al.* [21]; divided symbols, data from Zhu *et al.* [9]. Lines, present dCTMC calculation: solid line for (1,1); dashed line (1,2) & (2,1); dot-dashed line (1,3) & (3,1); and dotted line (>2, >2).

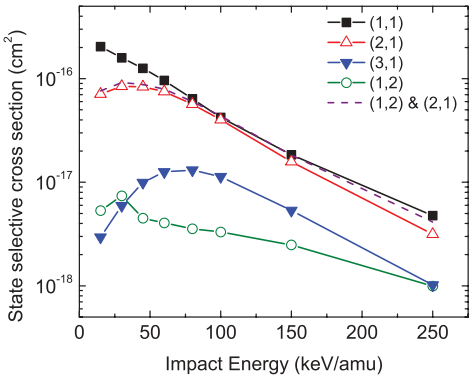

FIG. 3. (Color online) dCTMC state-selective capture cross sections as a function of impact energy.

mechanisms: (1,⩾2), (⩾2,1), & (⩾2,⩾2). When the reaction products are symmetric, as for the (1,2) and (2,1) channels, the experimental separation of those channels is not feasible and they add up together [(1,2) & (2,1)] as shown in Fig. 1.

The resolution of our apparatus for the longitudinal momentum component is 0.8 ± 0.2 a.u. (full width at half maximum). This resolution can be estimated from the target size and the detector resolution [26] and allows us to separate only the (1,1) channel from those involving excited states at any or both of the final reactants.

State-selective cross sections were then obtained by fitting the longitudinal momentum distributions shown in Fig. 1 by means of Gaussian functions. These values are listed in Table I and explicitly shown in Fig. 2 as a function of the impact energy. The experimental data from Mergel *et al.* [21] and Zhu *et al.* [9] are included and are seen to match the present data at the very edges of our energy range within the associated error bars. Concerning the theoretical data, Mergel *et al.* found dCTMC results to be in agreement with their data for impact energies in the range 60–250 keV/amu. The present dCTMC calculations are in agreement with theirs and have been extended to the lower impact energies here explored. The (1,2) & (2,1) channel is well described in the whole energy range, but for impact energies below 60 keV/amu, the (1,1) channel seems to be overestimated while the (1,⩾3) & (⩾3,1) channel is underestimated. This could be due to the microcanonical radial distribution employed which may not properly reproduce the quantum mechanical radial distributions. However, there still remains the lack of angular correlation between the electrons in the theoretical model. Such correlation is expected to play an increasing role as the impact energy is decreased, since all the collision partners strongly interact with each other for a longer period of time.

In spite of our qualitative agreement, we now infer the main physical trends that emerge from the theoretical state-selective data. In Fig. 3 we plot the separate contributions from the (1,1), (1,2), (2,1), and (3,1) channels predicted by the dCTMC model, many of which cannot be experimentally resolved. We observe that the (2,1) channel is clearly dominant over the (1,2) channel. A closer inspection of the range of impact parameters contributing to the (1,2) and (2,1) channels clearly shows that these channels are being fed from different ranges of impact parameters. The (2,1) channel is populated over a range of impact parameters larger than that associated with the (1,2) channel. The contribution of the (3,1) channel to the capture cross section is also larger than the (1,2) in most of the energy range explored. Interestingly, the relative contributions from these two channels seem to invert at approximately 250 keV/amu. This would probably indicate that at large impact energies the capture process becomes focused to the inner impact parameters for which the chance of getting target excitation turns dominant over electron capture to excited states with $n > 2$.

The total cross sections as functions of the projectile energy are shown in Fig. 4. These cross sections have been determined, for the present measurements, by normalization to the published total cross sections from Dubois [16,17]. The dCTMC total cross sections are in good agreement with the present data, as well as with those from Refs. [10–12] but tend to overestimate the experiment in the lower edge of the

TABLE I. Present experimental state-selective cross sections for $^3He^{2+}$+He collisions (in units of 10^{-16} cm^2).

	Energy (keV/amu)						
Final state (n,n')	13.3	20	25	33.3	50	66.67	100
(1,1)	0.3875	0.6880	0.6701	0.7120	0.7740	0.6607	0.3329
(1,2) & (2,1)	0.7920	1.1155	1.2101	1.2388	1.0070	0.8867	0.4548
(1,⩾3) & (3,1)	0.1765	0.5580	0.7256	0.7954	0.6890	0.5590	0.1734
(⩾2, ⩾2)	0.0140	0.0180	0.0240	0.0340	0.0494	0.0536	0.0340

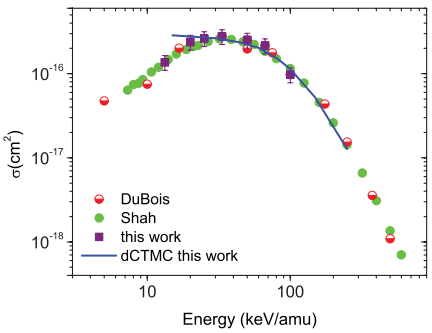

FIG. 4. (Color online) Total cross sections for single charge exchange. Experimental data used for normalization: solid circles, Shah *et al.* [14,15]; partially filled circles, DuBois *et al.* [16,17], solid squares, this work, showing the location used for normalization. Solid line, present dCTMC calculation.

energy range explored, a trend that can also be inferred from observation of Fig. 2.

To summarize, in this work we have shown state-selective and total cross sections for single charge exchange in $^3He^{2+}$ collisions with helium targets at intermediate impact energies. The present data covers an experimentally unexplored energy range that perfectly suits the range of operation of our Kevatron accelerator.

In the impact energy range explored, we found that the associated (1,2) & (2,1) channels were dominant over the (1,1) channel and the (1,$\geqslant$3) & ($\geqslant$3,1) channels. These data are in qualitative agreement with the present dCTMC results, although we note that the agreement improves for impact energies larger than 60 keV/amu. Capture to excited states of the projectile together with simultaneous target excitation ($\geqslant$2,$\geqslant$2) provides, on the other hand, a minor contribution to the single-capture total cross section compared to the other channels.

At the very edges of the energy range of the Kevatron our state-selective data match closely those from the Frankfurt and Lanzhou groups, giving confidence to the novel COLTRIMS facility at the Centro Atómico Bariloche.

Work at Centro Atómico Bariloche supported by CNEA (Argentina). Work at UNS supported by Grants No. PGI 24/F049 and No. PICT-2007-00887 of the ANPCyT and Grant No. PIP 112-200801-02760 of CONICET (Argentina). Useful discussions with J. Fiol, D. Fregenal, G. Bernardi, O. Jagutzki, Klaus Ullmann-Pfleger, M. Schöffler, and W. Wolff are gratefully acknowledged.

[1] T. Kambara *et al.*, J. Phys. B **28**, 4593 (1995).
[2] R. Moshammer, M. Unverzagt, W. Schmitt, J. Ullrich, and H. Schmidt-Böcking, Nucl. Instrum. Meth. Phys. Res. B **108**, 425 (1996).
[3] A. Cassimi, S. Duponchel, X. Flechard, P. Jardin, P. Sortais, D. Hennecart, and R. E. Olson, Phys. Rev. Lett. **76**, 3679 (1996).
[4] J. Ullrich, R. Moshammer, R. Dörner, O. Jagutzki, V. Mergel, H. Schmidt-Böcking, and L. Spielberger, J. Phys. B **30**, 2917 (1997).
[5] M. Abdallah, C. L. Cocke, S. Kravis, E. C. Montenegro, R. Moshammer, L. Saleh, J. Ullrich, S. L. Varghese, W. Wolff, and H. Wolf, Appl. Accel. Res. Ind. AIP **392**, 209 (1997).
[6] R. Dörner, V. Mergel, O. Jagutzki, L. Spielberger, J. Ullrich, R. Moshammer, and H. Schmidt-Böcking, Phys. Rep. **330**, 95 (2000).
[7] J. Ullrich, R. Moshammer, A. Dorn, R. Dörner, L. Ph. H. Schmidt, and H. Schmidt-Böcking, Rep. Prog. Phys. **66**, 1463 (2003).
[8] C. L. Cocke, Phys. Scr. T **110**, 9 (2004).
[9] X. L. Zhu *et al.*, Chin. Phys. Lett. **23**, 587 (2006).
[10] R. Dörner *et al.*, Phys. Rev. A **57**, 1074 (1998).
[11] D. Fischer, R. Moshammer, M. Schultz, A. Voitkiv, and J. Ullrich. J. Phys. B **36**, 3555 (2003).
[12] T. Havermeier *et al.*, Phys. Rev. Lett. **104**, 153401 (2010).
[13] V. V. Afrosimov, A. A. Basalaev, G. A. Leiko, and M. N. Panov, Sov. Phys. JETP **47**, 5 (1978).
[14] M. B. Shah and H. B. Gilbody, J. Phys. B **18**, 899 (1985).
[15] M. B. Shah, P. McCallion, and H. B. Gilbody, J. Phys. B **22**, 3037 (1989).
[16] R. D. DuBois, Phys. Rev. A **33**, 1595 (1986).
[17] R. D. DuBois, Phys. Rev. A **36**, 2585 (1987).
[18] H. O. Folkerst, R. Hoekstra, L. Meng, R. E. Olson, W. Fritsch, R. Morgenstern, and H. P. Summers, J. Phys. B **26**, L619 (1993).
[19] R. Dörner *et al.*, Nucl. Instrum. Methods Phys. Res. B **99**, 111 (1995).
[20] M. S. Schöffler, J. N. Titze, L. Ph. H. Schmidt, T. Jahnke, O. Jagutzki, H. Schmidt-Böcking, and R. Dörner, Phys. Rev. A **80**, 042702 (2009).
[21] V. Mergel *et al.*, Phys. Rev. Lett. **74**, 2200 (1995).
[22] V. G. Hasan, S. Knoop, R. Morgenstern, and R. Hoekstra, J. Phys. Conf. Ser. **58**, 199 (2007).
[23] M. S. Schöffler, J. Titze, L. Ph. H. Schmidt, T. Jahnke, N. Neumann, O. Jagutzki, H. Schmidt-Böcking, R. Dörner, and I. Mančev, Phys. Rev. A **79**, 064701 (2009).
[24] RoentDek Handels GmbH. [http://www.roentdek.com].
[25] W. C. Wiley and I. H. McLaren, Rev. Sci. Instr. **26**, 1150 (1955).
[26] M. Alessi, D. Fregenal, and P. Focke, Nucl. Instrum. Methods Phys. Res. B (in press).
[27] Th. Weber *et al.*, Phys. Rev. Lett. **86**, 224 (2001).
[28] R. E. Olson, Phys. Rev. A **36**, 1519 (1987).
[29] M L. McKenzie and R. E. Olson, Phys. Rev. A **35**, 2863 (1987).
[30] A. E. Wetmore and R. E. Olson, Phys. Rev. A **38**, 5563 (1988).
[31] V. J. Montemayor and G. Schiwietz, Phys. Rev. A **40**, 6223 (1989).
[32] L. Meng, R. E. Olson, R. Dörner, J. Ullrich, and H. Schmidt-Böcking, J. Phys. B **26**, 3387 (1993).
[33] R. Becker and A. D. McKellar, J. Phys. B **17**, 3923 (1984).